# Supporting Information

## Non-Precious Bimetallic Iron-Molybdenum Sulfide Electrocatalysts for Hydrogen Evolution Reaction in Proton-Exchange Membrane Electrolyzers

*Adina Morozan*[✧,#], *Hannah Johnson*[§,#], *Camille Roiron*[✧], *Ghislain Genay*[✧], *Dmitry Aldakov*[⊡], *Ahmed Ghedjatti*[✧], *Chuc T. Nguyen*[△], *Phong D. Tran*[△], *Sachin Kinge*[§], *Vincent Artero*[✧,*]

[✧]Univ. Grenoble Alpes, CNRS, CEA/IRIG, Laboratoire de Chimie et Biologie des Métaux, 17 rue des Martyrs, 38054 Grenoble, France

[§]Toyota Motor Europe, Advanced Technology, Hoge Wei 33, Zaventem 1930, Belgium

[⊡]Univ. Grenoble Alpes, CNRS, CEA/IRIG, SyMMES, STEP, 17 rue des Martyrs, 38054 Grenoble, France

[△]University of Science and Technology of Hanoi, Vietnam Academy of Science and Technology, 18 Hoang Quoc Viet, Ha Noi, Vietnam

[*]Correspondig author: vincent.artero@cea.fr

[#]These authors contributed equally.

This information is available free of charge on the ACS Publications website.

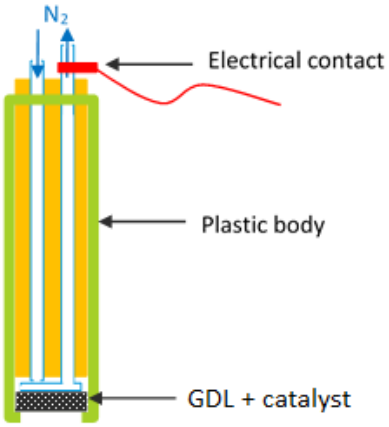


**Figure S1**. The half-cell holder for gas diffusion electrode (GDE) setup; GDE is composed from a GDL and a drop casted catalyst layer.

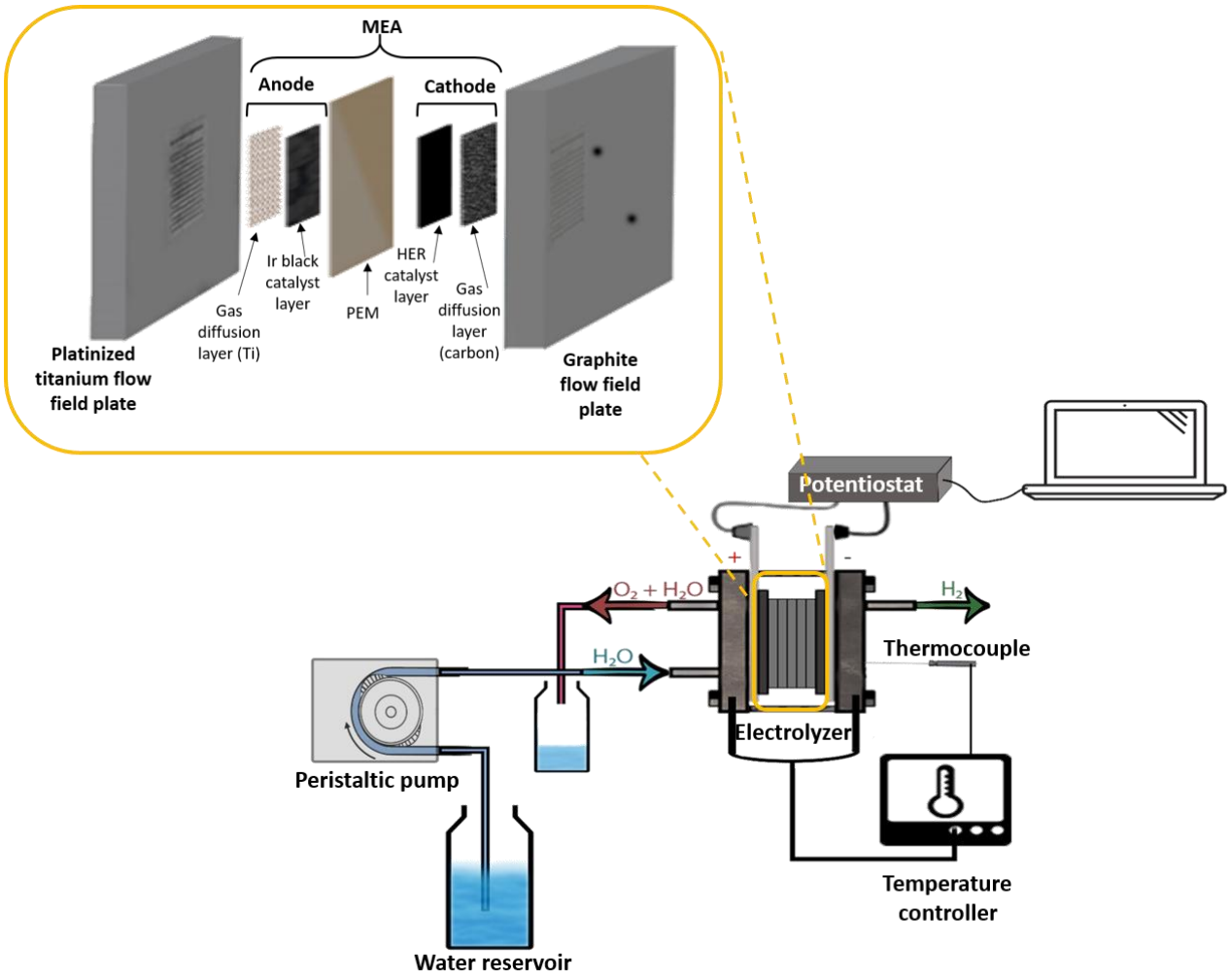


**Figure S2**. PEM electrolyzer setup

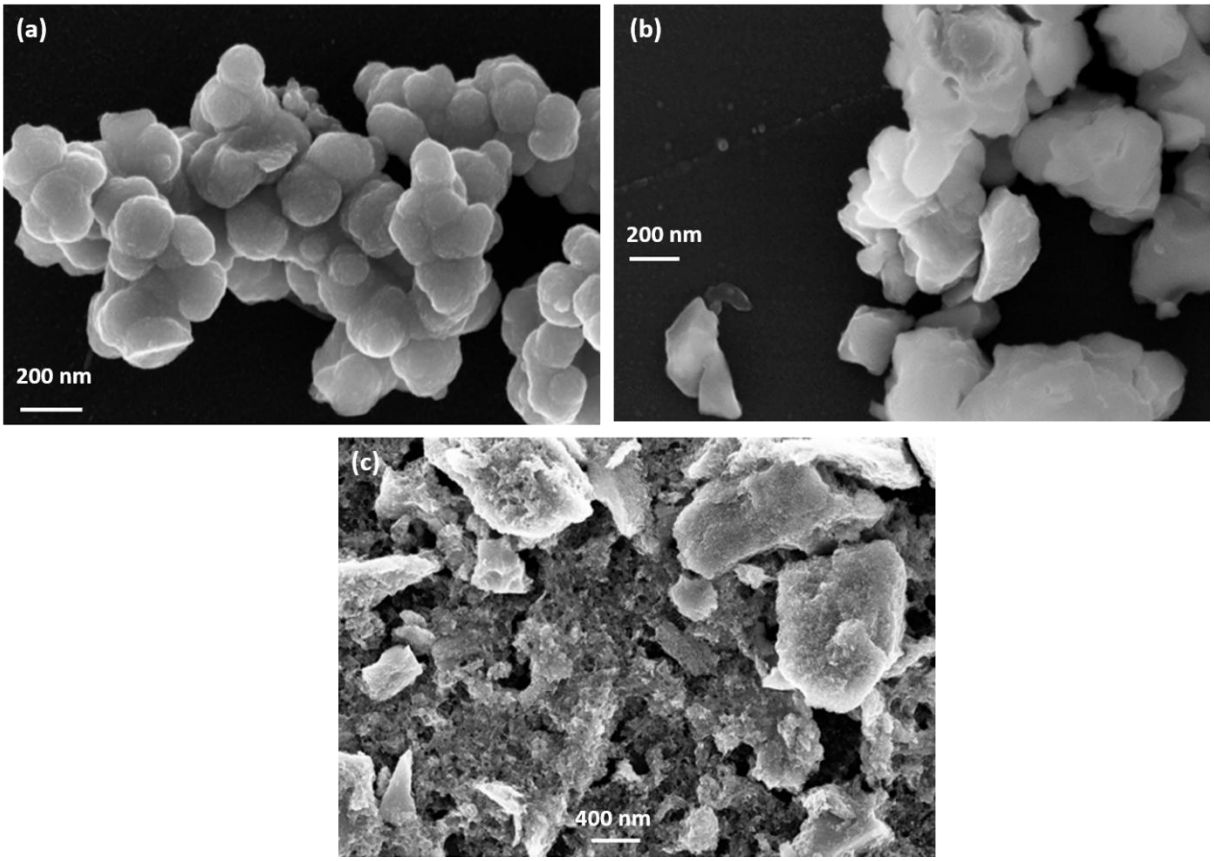


**Figure S3**. SEM images of (a) $MoS_{(mw)}$, (b) $MoS_{(HT, Ar)}$ and (c) $MoS_{(HT, Ar+H_2)}$.

The $MoS_{(mw)}$ sample (Figure S3a) is made up of particle self-assemblies of spherical shape with an average diameter around 100 nm. $MoS_{(HT, Ar)}$ and $MoS_{(HT, Ar+H_2)}$ samples (Figure S3b and 3c) present an irregular shape and micrometer size particles, and $MoS_{(HT, Ar)}$ reveals a smoother surface.

**Preparation of a-$MoS_x$ nanoparticles via chemical oxidation of $[MoS_4](NH_4)_2$**

We describe here the synthesis of the amorphous molybdenum sulfide (a-$MoS_x$) via chemical oxidation as previously reported in reference [1]. We refer to this material (a-$MoS_x$) when discussing the Raman spectra (Figure S4) of our molybdenum sulfides materials obtained by microwave irradiation and heat treatment. As detailed below, this comparison highlights the differences and similarities to the reported coordination polymer amorphous phase in the reference [1].

*Synthesis:* Sodium persulfate (2 mmol, 480 mg) was added to a deep-red solution of $[MoS_4](NH_4)_2$ (1 mmol, 260 mg) in water (50 ml) well degassed with Ar. The solution rapidly turned to a dark brown suspension which was continuously stirred under Ar for 2 h. When the reaction was over, a

dark brown powder was collected by centrifugation, and thoroughly washed with water, ethanol, and diethyl ether. This product was dried under vacuum.[1]

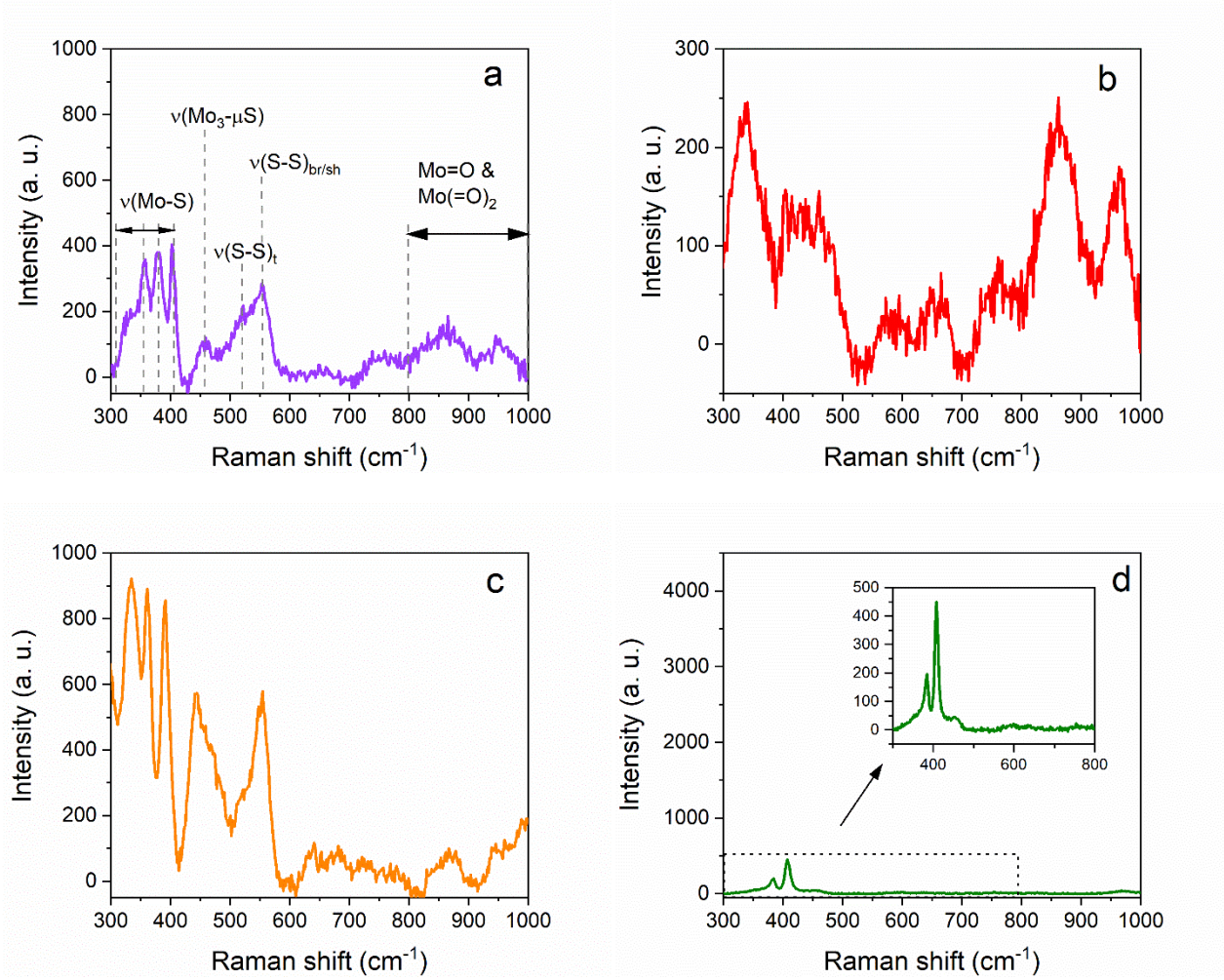


**Figure S4**. Raman spectra (532 nm green laser excitation with low power 0.5 mW) of (a) a-$MoS_x$, (b) $MoS_{(mw)}$, (c) $MoS_{(HT, Ar)}$ and (d) $MoS_{(HT, Ar+H_2)}$.

In the amorphous molybdenum sulfide (a-$MoS_x$) prepared via chemical oxidation[1] (Figure S4a), peaks from bridging and sharing disulfide ligands $\nu(S{-}S)_{br/sh}$ were found at 555 $cm^{-1}$, while terminal disulfide ligand $\nu(S{-}S)_t$ were found at 520 $cm^{-1}$. Mo−S bonds were characterized by typical molybdenum sulfide vibration mode of $\nu(Mo_3{-}\mu S)$ at 455 $cm^{-1}$ and $\nu$(Mo−S) at 400−300 $cm^{-1}$, respectively.[1-2]

The Raman spectrum (Figure S4b) indicates the amorphous nature of the $MoS_{(mw)}$ is significantly different from the reported coordination polymer amorphous phase made of $[Mo_3S_{13}]^{2-}$ discrete

building blocks[1]. A further evidence of this assumption is the lack of extrusion of $[Mo_3S_{13}]^{2-}$ clusters from $MoS_{(mw)}$ material as reported in ref. [1], a complete dissolution of $MoS_{(mw)}$ in concentrated NaOH solution leading to concluding a lack of such clusters by microwave synthesis. The Raman features at 800-1000 $cm^{-1}$ have assigned to molybdenum oxides defects[1] as well as to possible presence of molybdenum oxysulfide $MoS_xO_y$.[3]

The structure of the molybdenum sulfides obtained by heat treatment depending on the flowing atmosphere used during heat treatment, evolving from amorphous to crystalline by changing the Ar atmosphere to the reducing,mixed ($Ar+H_2$) atmosphere.

The $MoS_{(HT,\ Ar)}$ sample (Figure S4c) shows Raman signatures typical to polymer amorphous molybdenum sulfide[1-2] but less well-defined, without a proper local structure. This could be due to the different polymerization level and/or the presence of more binuclear Mo species than $[Mo_3S_{13}]^{2-}$ clusters.

The characteristics vibrations of crystalline molybdenum sulfide at 382 $cm^{-1}$ ($E^1_{2g}$) and 406 $cm^{-1}$ ($A_{1g}$) occur consistent with the formation of the crystalline phase in the $MoS_{(HT,\ Ar+H_2)}$ sample (Figure S4d).[4]

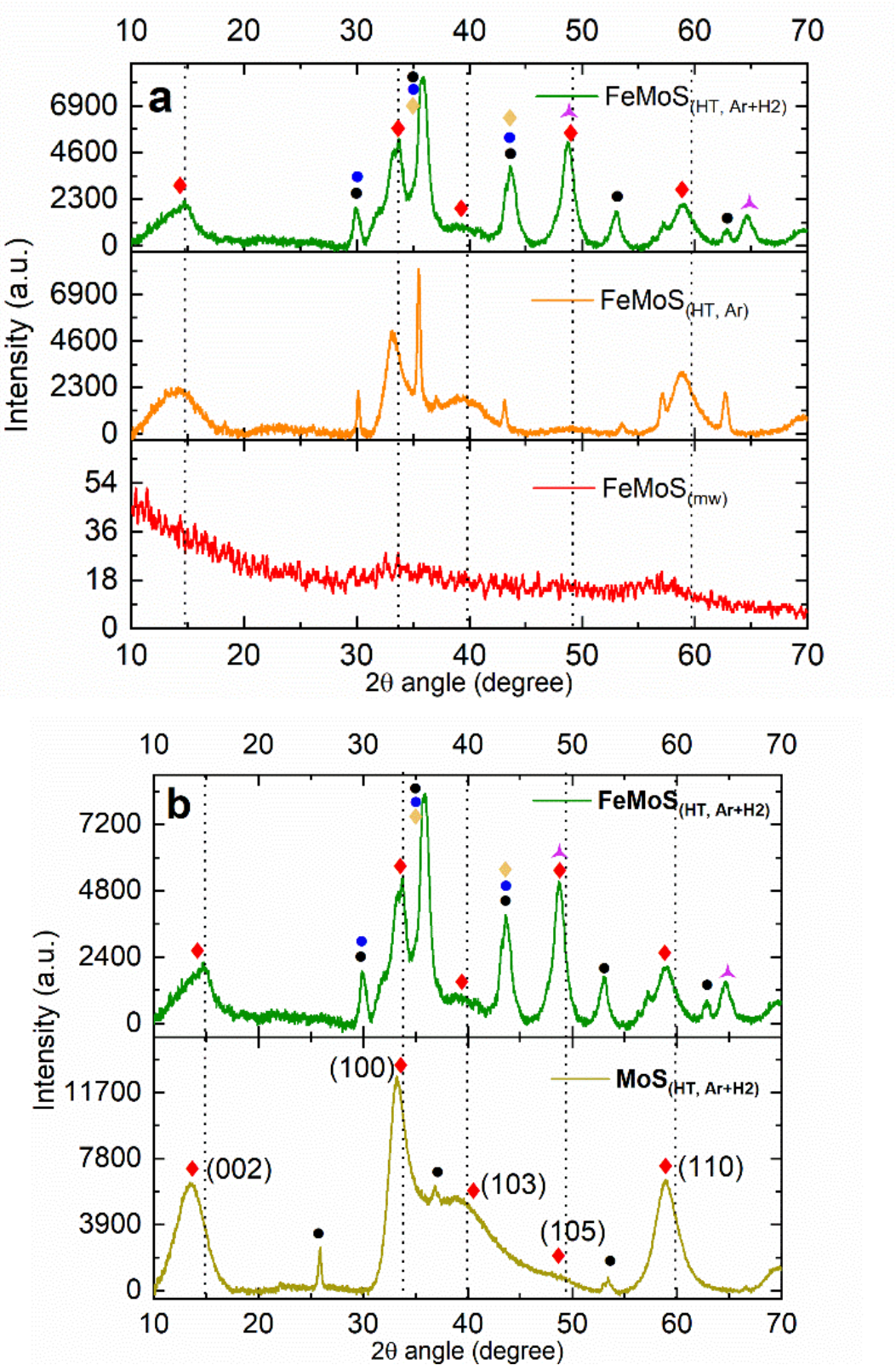


**Figure S5**. X-ray diffraction (XRD) patterns recorded for the different materials synthesized in this study. The different peaks are assigned with the following symbols according to previous literature: ♦ c-$MoS_2$;[5-8] • Mo-oxides and • Mo, Fe-oxides;[9-10] ♦ Fe, Mo-sulfide; [11] ⅄ Fe-sulfides[12]

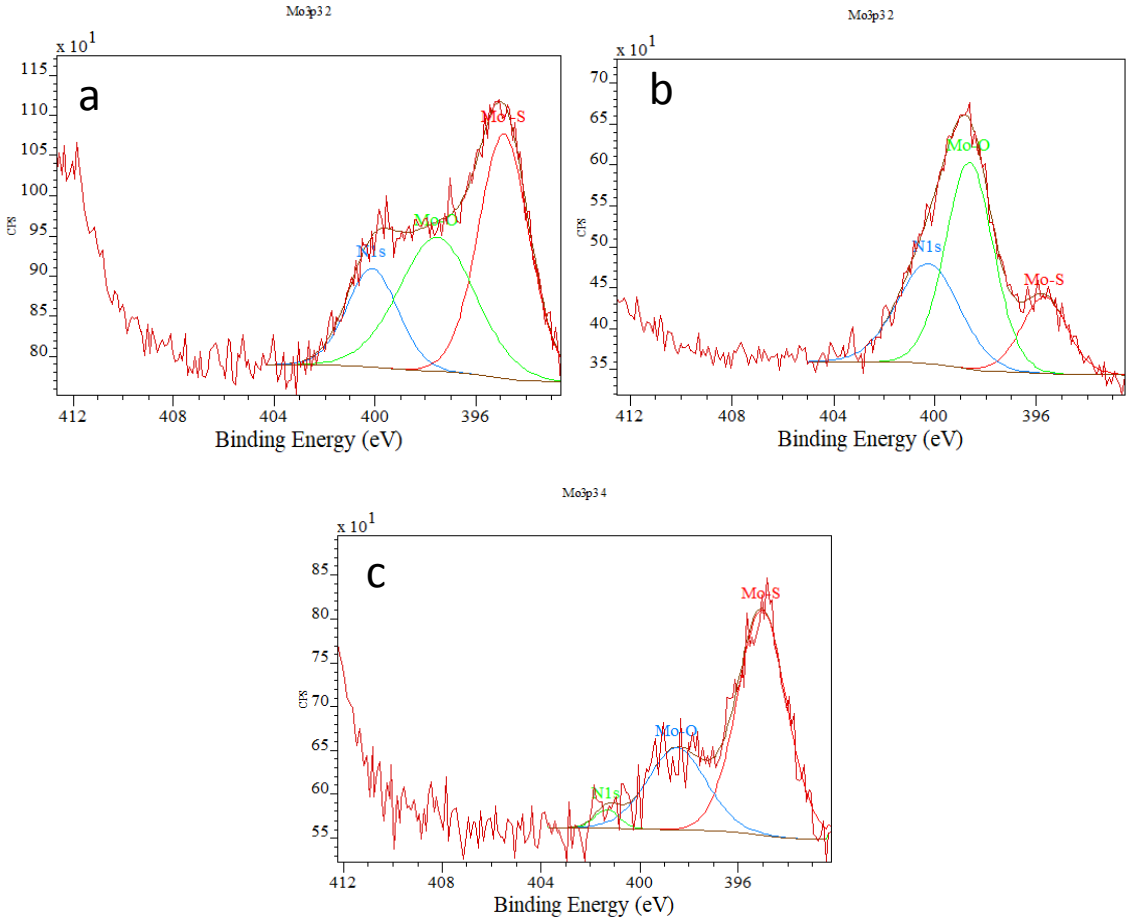


**Figure S6**. XPS spectra of Mo 3p region of $MoS_{(mw)}$ (a), $MoS_{(HT, Ar)}$ (b), $MoS_{(HT, Ar+H_2)}$ (c).

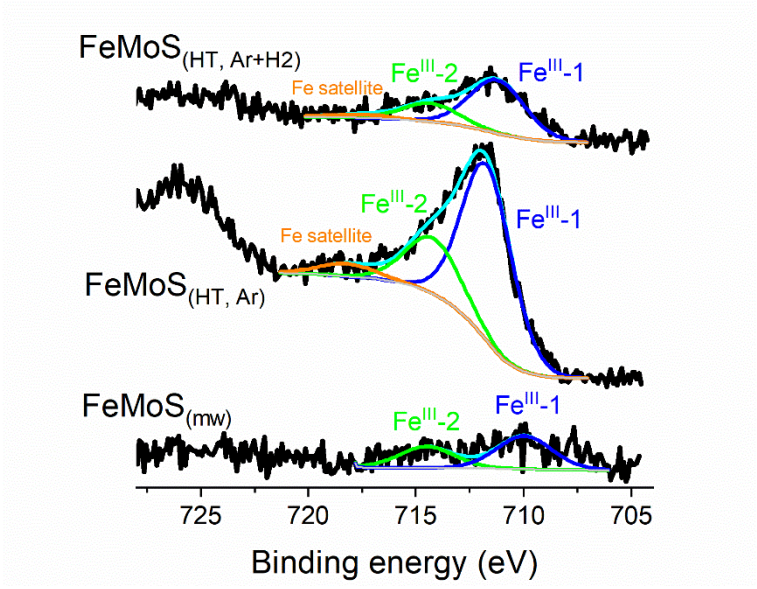


**Figure S7**. X-ray photoelectron spectroscopy (XPS) spectra of Fe2p.

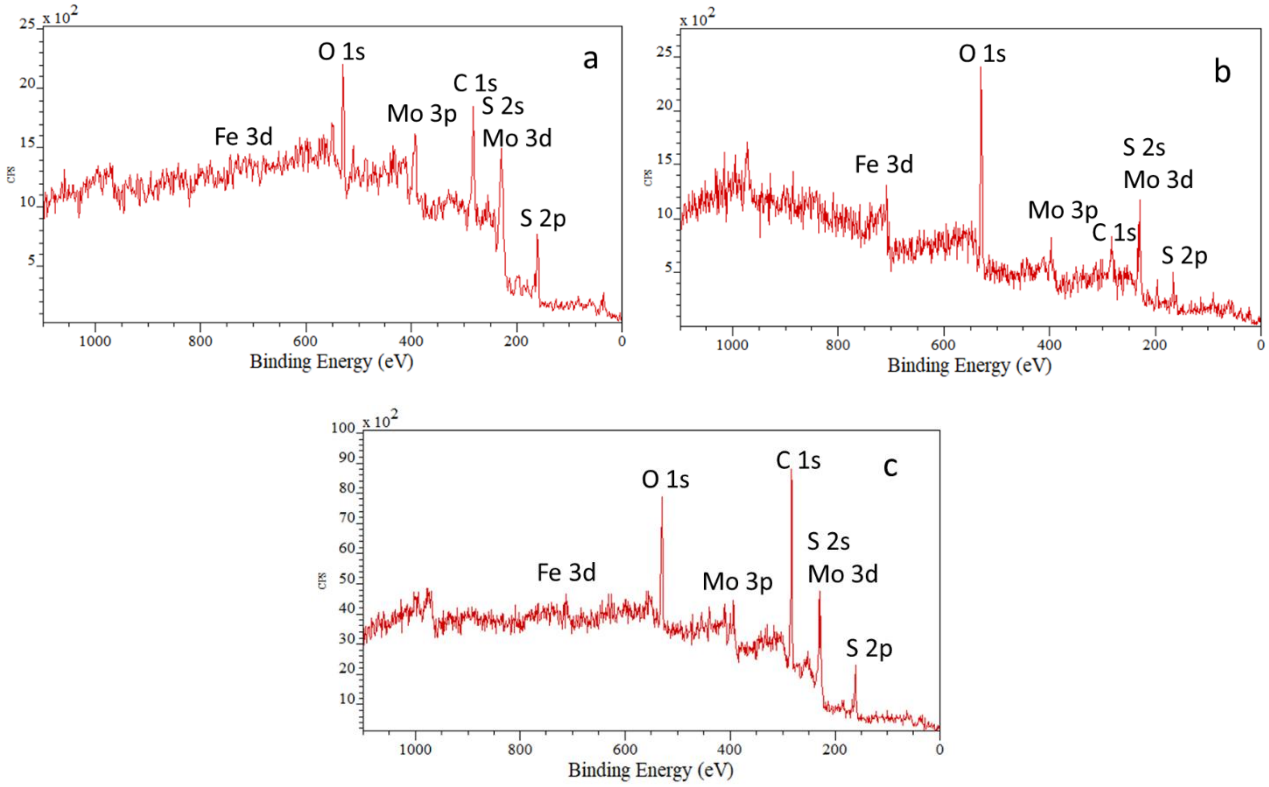


**Figure S8**. XPS survey spectra of $MoS_{(mw)}$ (a), $MoS_{(HT, Ar)}$ (b), $MoS_{(HT, Ar+H_2)}$ (c).

## Determination of the electrochemically active surface area (ECSA) from CV measurements in $K_3[Fe(CN)_6]$

The ECSA was estimated by cyclic voltammetry using ferricyanide as a redox probe.[13-15] The cyclic voltammograms (CVs) were recorded at various scan rates (e.g., ν = 10, 20, 40, 60, 80 and 100 $mV \cdot s^{-1}$) in 10 mM $K_3[Fe(CN)_6]$ with 0.1 M KCl as supporting electrolyte, under nitrogen degassed atmosphere. The applied potential ranged between –0.1 and 0.5 V vs Ag/AgCl reference electrode with a Pt counter electrode. The working electrode was a GC electrode (∅ = 3 mm, 0.07 $cm^2$) with a drop casted electrocatalyst layer. A catalyst ink including 1 mg of electrocatalyst, 80 µL of ethanol, 20 µL of water, 5 µL of 5 wt. % Nafion solution was prepared by sonication. Then, 4 µl of the ink were deposited on the GC disk to reach a catalyst loading of 0.55 $mg \cdot cm^{-2}$.

Figure S9 displays a series of CVs on the GC/catalyst electrode. The peak reduction current ($I_p$) was plotted as a function of the square root of the potential scan rate ($\nu^{1/2}$). The dependence of the peak current on the scan rate is described by the Randles-Sevcik equation at room temperature (1):

$$I_p = (2.69 \times 10^5) n^{3/2} A C D^{1/2} \vartheta^{1/2} \quad (1)$$

where:

**$I_p$** is the reduction peak intensity of the redox couple illustrated in Figure S9 (mA)

**n** is the number of electrons involved in the reaction (n = 1 for $[Fe(CN)_6^{3-}]$ / $[Fe(CN)_6^{4-}]$)

**A** is the active area ($cm^2$)

**C** is the concentration of the bulk solution, $K_3[Fe(CN)_6]$ ($mol \cdot L^{-1}$)

**ν** is the scan rate ($V \cdot s^{-1}$)

**D** is the diffusion coefficient of $Fe(CN)_6^{3-}$ ($cm^2 \cdot s^{-1}$)

The ECSA can be calculated from the value of the **slope = $I_p/\nu^{1/2}$**, since n, C, D are constant values. The diffusion coefficient of $Fe(CN)_6^{3-}$ (10 mM $K_3[Fe(CN)_6]$ in 0.1 M KCl) was determinated experimentally [15] in this study and found to be $3.85 \times 10^{-6}$ $cm^2 \cdot s^{-1}$.

**Table S1.** ECSA values of the as-synthesized materials

| **Catalyst** | **slope = $I_p/\nu^{1/2}$** | **ECSA ($cm^2$)** |
|---|---|---|
| $FeMoS_{(mw)}$ | 0.157 | $2.7 \times 10^{-2}$ |
| $MoS_{(mw)}$ | 0.064 | $1.1 \times 10^{-2}$ |
| $FeMoS_{(HT, Ar)}$ | 0.022 | $0.38 \times 10^{-2}$ |
| $MoS_{(HT, Ar)}$ | 0.057 | $0.98 \times 10^{-2}$ |
| $FeMoS_{(HT, Ar+H2)}$ | 0.017 | $0.29 \times 10^{-2}$ |
| $MoS_{(HT, Ar+H2)}$ | 0.037 | $0.64 \times 10^{-2}$ |

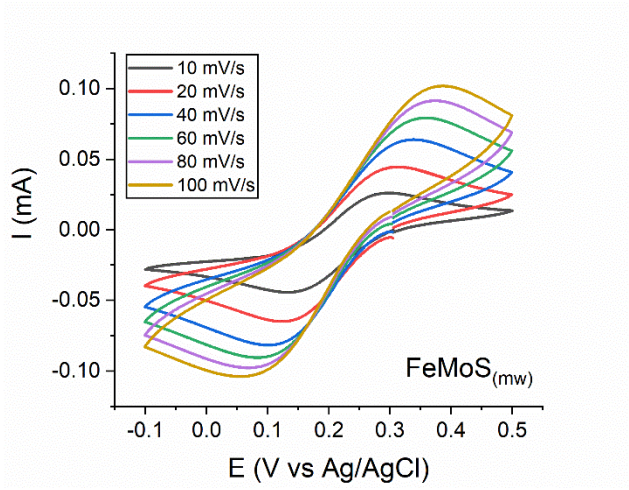
10 mV/s
20 mV/s
40 mV/s
60 mV/s
80 mV/s
100 mV/s
I (mA)
E (V vs Ag/AgCl)
FeMoS(mw)

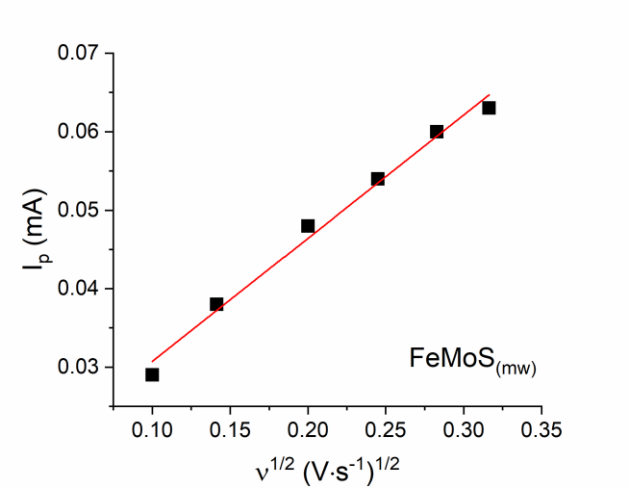
Ip (mA)
ν1/2 (V·s-1)1/2
FeMoS(mw)

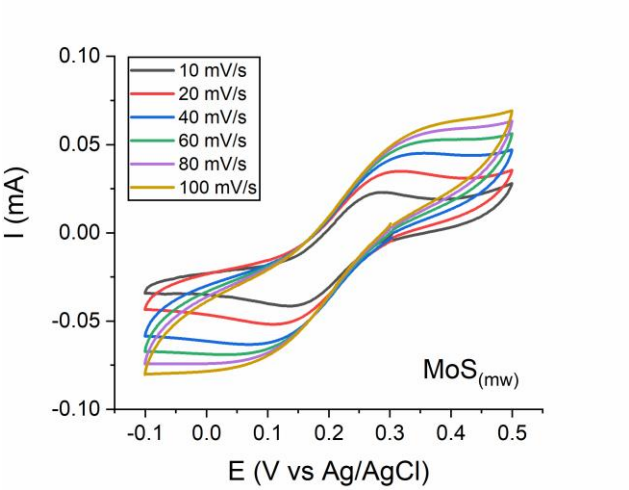
10 mV/s
20 mV/s
40 mV/s
60 mV/s
80 mV/s
100 mV/s
I (mA)
E (V vs Ag/AgCl)
MoS(mw)

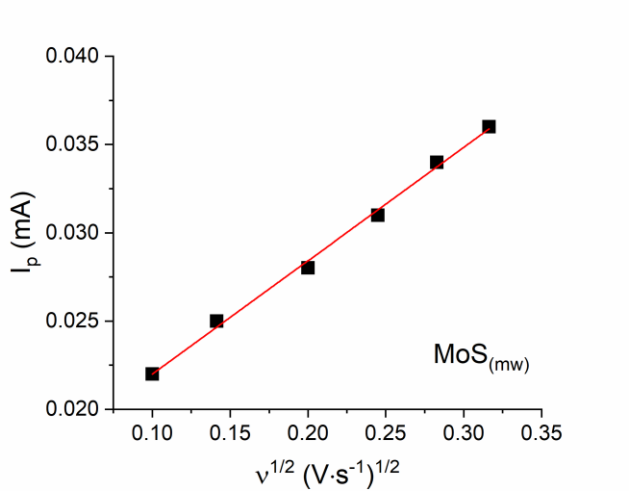
Ip (mA)
ν1/2 (V·s-1)1/2
MoS(mw)

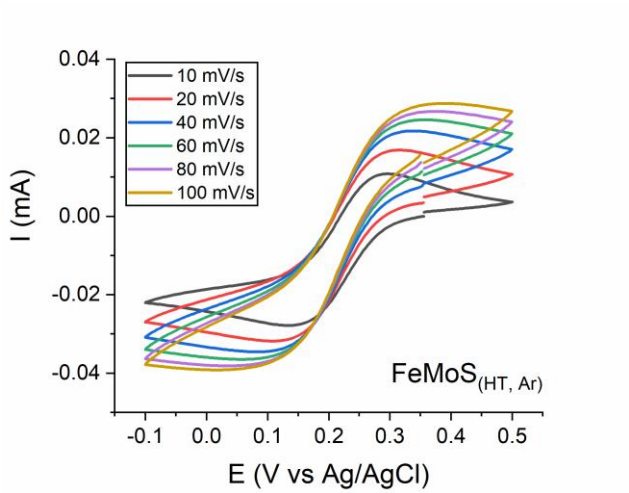
10 mV/s
20 mV/s
40 mV/s
60 mV/s
80 mV/s
100 mV/s
I (mA)
E (V vs Ag/AgCl)
FeMoS(HT, Ar)

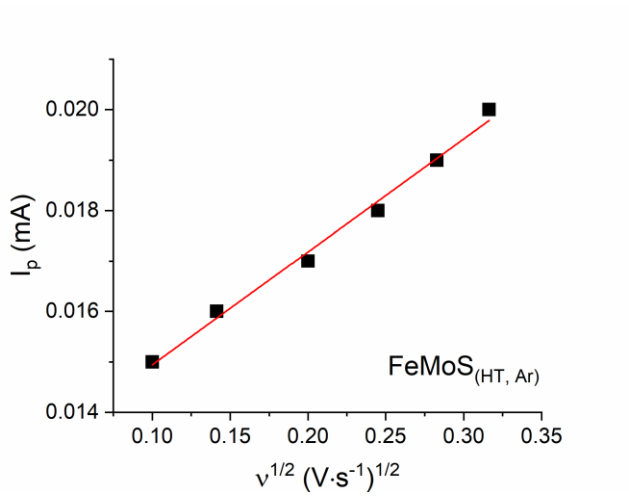
Ip (mA)
ν1/2 (V·s-1)1/2
FeMoS(HT, Ar)

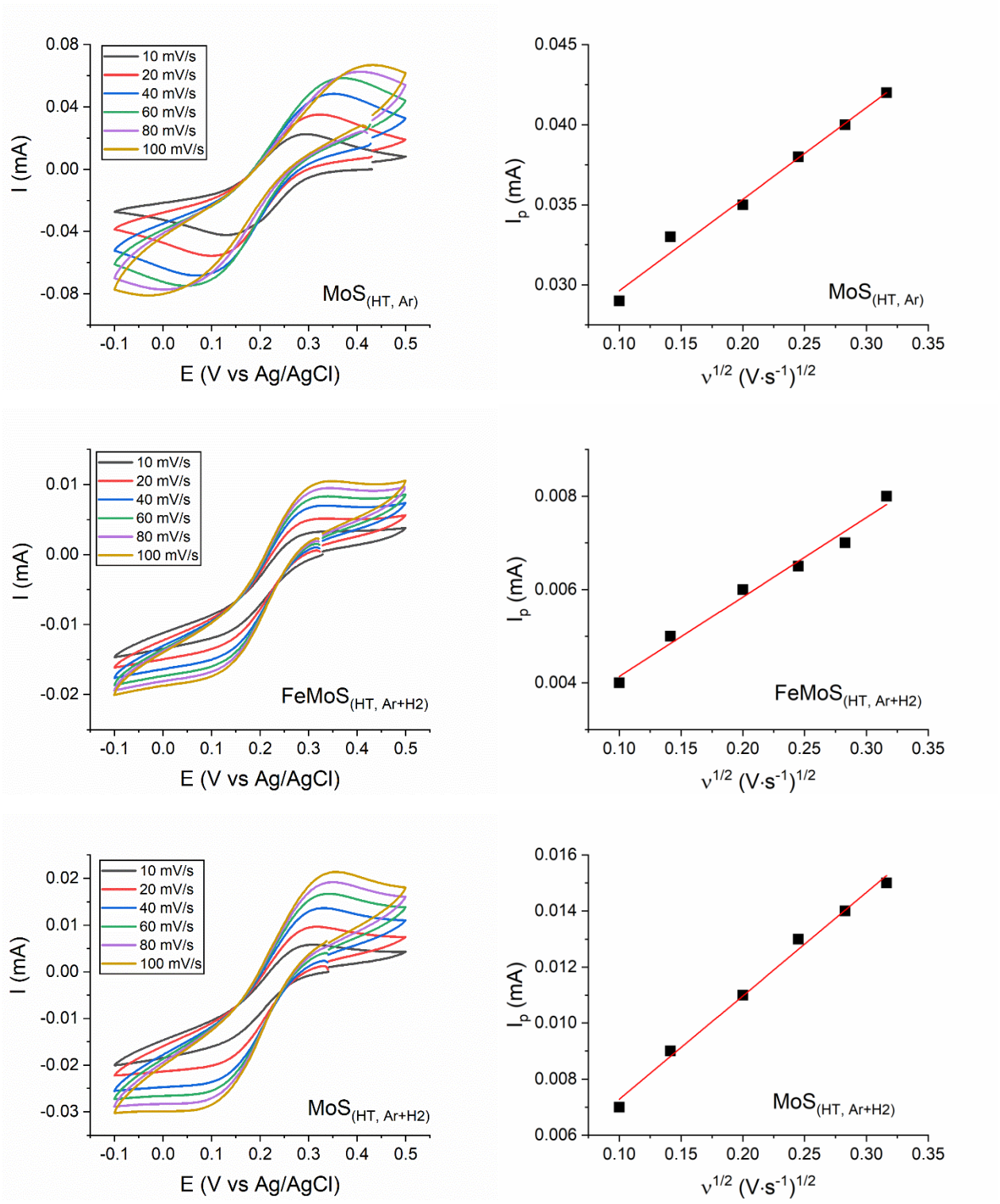


**Figure S9**. Cyclic voltammograms and peak currents as a function of scan rate on the GC/catalyst electrodes in degassed 10 mM $K_3[Fe(CN)_6]$ with 0.1 M KCl as supporting electrolyte at different scan rates.

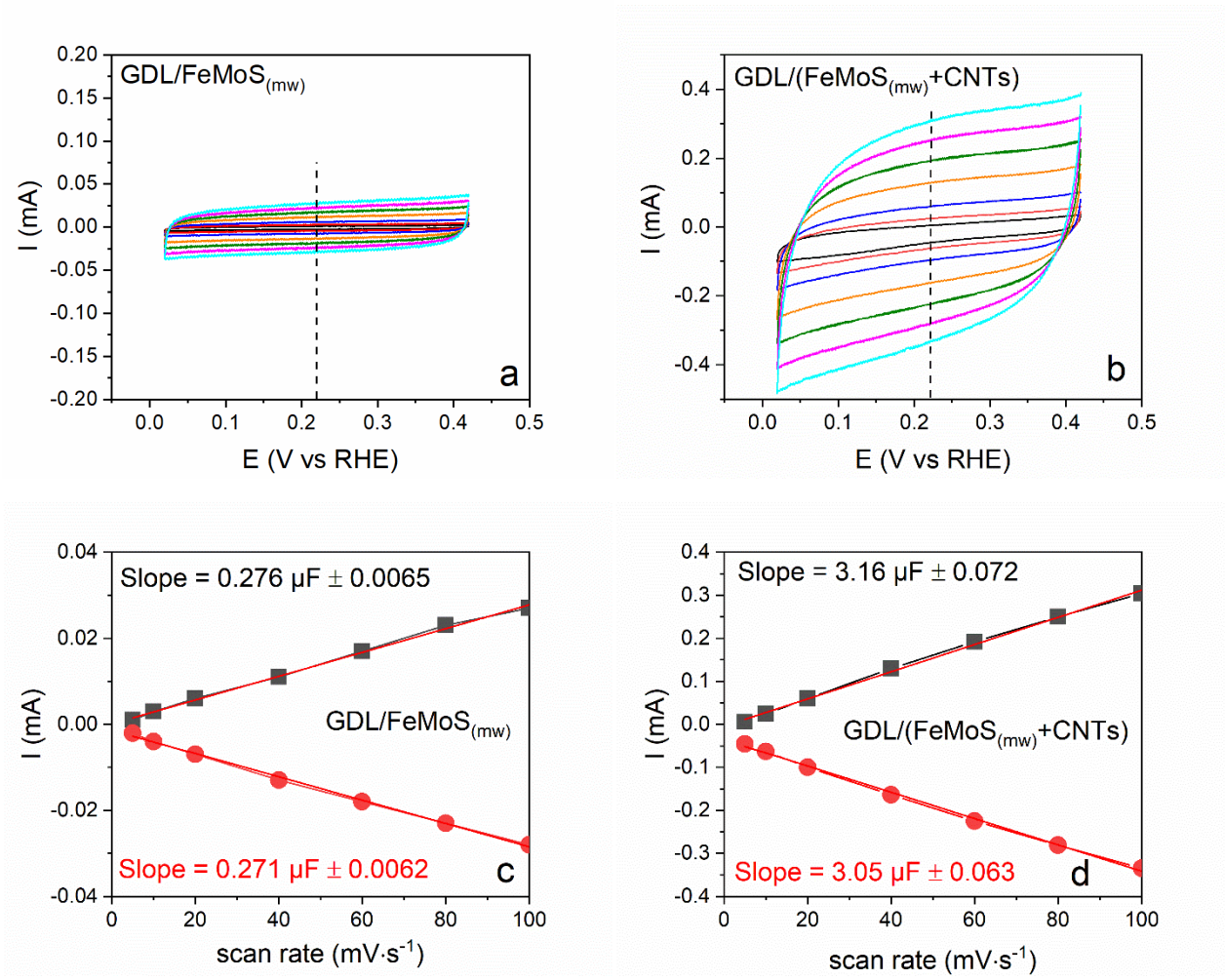


**Figure S10**. Double-layer capacitance measurements for determining electrochemically-active surface area of GDL/$FeMoS_{(mw)}$ and GDL/($FeMoS_{(mw)}$+CNTs) electrodes (catalyst loading: 0.24 mg·$cm^{-1}$). (a, b) Cyclic voltammograms were measured in a non-Faradaic region of the voltammogram at the following scan rate: (—) 5, (—) 10, (—) 20, (—) 40, (—) 60, (—) 80, and (—) 100 mV/s. All current is assumed to be due to capacitive charging; (c, d) The cathodic (!) and anodic (,) charging currents measured at 0.22 V vs. RHE are plotted as a function of scan rate. The double-layer capacitance of the system is taken as the average of the absolute value of the slope of the linear fits to the data.

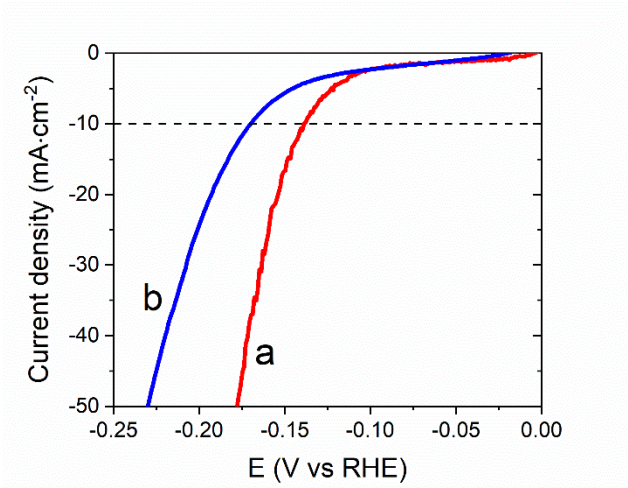


**Figure S11**. Polarization curves for HER on: (a). GDL/($FeMoS_{(mw)}$+CNTs) and (b). GDL/($MoS_{(mw)}$+CNTs); ($N_2$-saturated 0.5 M $H_2SO_4$, scan rate 5 $mV \cdot s^{-1}$, Ti wire counter electrode, catalyst loading 0.97 $mg \cdot cm^{-2}$)

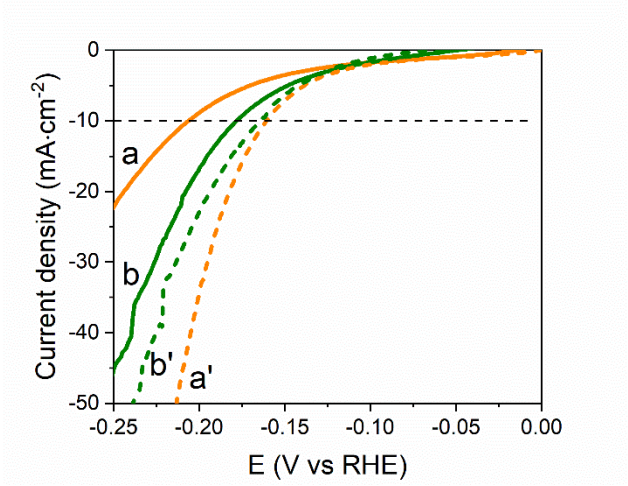


**Figure S12**. Polarization curves for HER on: (a). GDL/($FeMoS_{(HT,\ Ar)}$+CNTs), (a′). GDL/($MoS_{(HT,\ Ar)}$+CNTs), (b). GDL/($FeMoS_{(HT,\ Ar+H_2)}$+CNTs) and (b′). GDL/($MoS_{(HT,\ Ar+H_2)}$+CNTs); (0.5 M $H_2SO_4$, scan rate 5 $mV \cdot s^{-1}$, Ti wire counter electrode, catalyst loading 0.97 $mg \cdot cm^{-2}$)

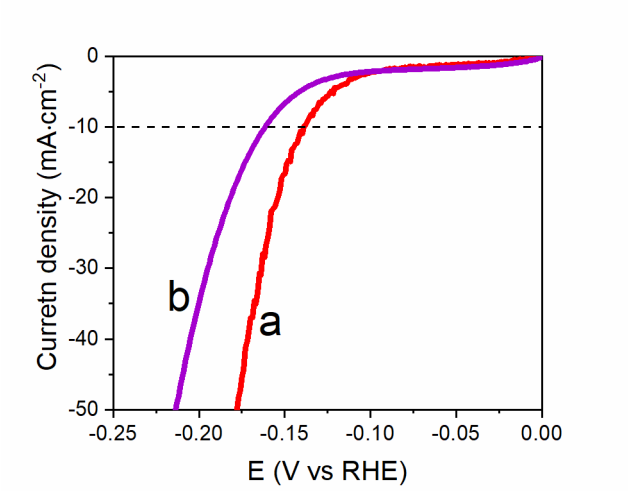


**Figure S13**. Polarization curves for HER corresponding to two electrode formulations with $FeMoS_{(mw)}$ electrocatalyst:

a). GDL/($FeMoS_{(mw)}$+CNTs) - catalyst loading 0.97 mg·cm$^{-2}$ and mass ratio catalyst:CNTs = 1:0.2, $\eta_{10}^{HER}$ = 140 mV

b). GDL/($FeMoS_{(mw)}$+Vulcan) - catalyst loading 0.97 mg·cm$^{-2}$ and mass ratio catalyst:Vulcan = 1:0.2, $\eta_{10}^{HER}$ = 160 mV

The Vulcan is a large surface area carbon black with high corrosion resistance and the most conductivity of commercially available carbon support.[16-17]

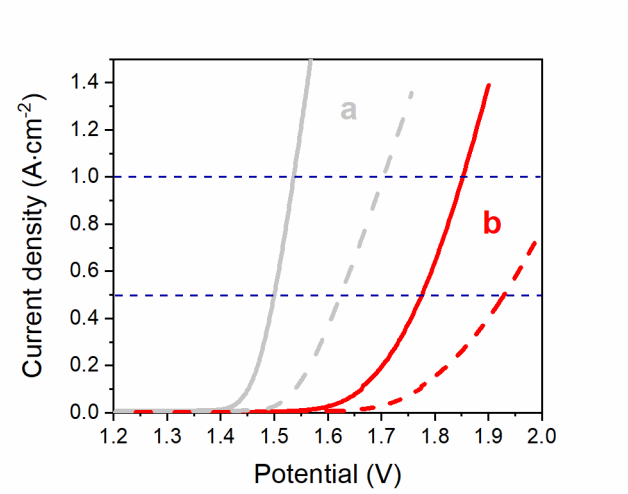


**Figure S14**. Single cell polarization curves for PEM electrolysis (80 °C, continuous line or RT, dashed line) using three distinct MEA: (a). Ir black/NRE-212/Pt-C and (b). Ir black/NRE-212/($FeMoS_{(mw)}$+Vulcan).

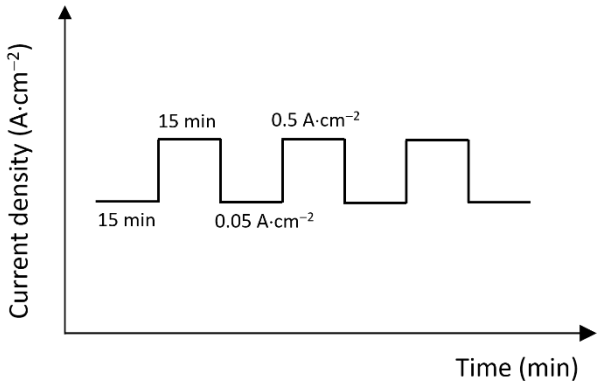


**Figure S15**. Graphical representation of the accelerated stress test (AST)

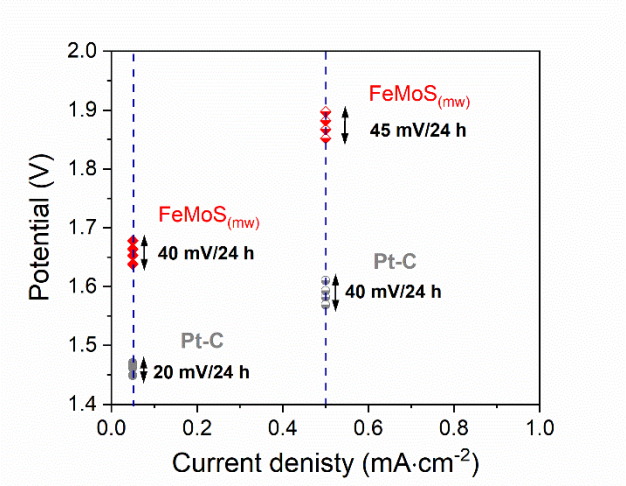


**Figure S16**. Performances of PEM electrolyzers (80 °C) with Pt-C (0.5 mg·cm$^{-2}$, in gray) or (FeMoS$_{(mw)}$+Vulcan) (4 mg·cm$^{-2}$, in red) as the HER catalysts and commercial Ir black (2 mg·cm$^{-2}$) as the OER catalyst: potential evolution (ΔE, mV) after 24 h-AST to reach 0.05 A·cm$^{-2}$ or 0.5 A·cm$^{-2}$

**Table S2.** Performances of PEM electrolyzers at RT and 80 °C

| Cathode catalyst | Curren density ($mA \cdot cm^{-2}$) | E (V) | | Reference |
|---|---|---|---|---|
| | | RT | 80 °C | |
| Pt-C | 0.05 | 1.52 | 1.44 | this work |
| | 0.1 | 1.54 | 1.45 | |
| | 0.5 | 1.62 | 1.50 | |
| | 1 | 1.70 | 1.54 | |
| $FeMoS_{(mw)}$+Vulcan | 0.05 | 1.72 | 1.63 | this work |
| | 0.1 | 1.77 | 1.66 | |
| | 0.5 | 1.93 | 1.77 | |
| | 1 | - | 1.85 | |
| $MoS_2$/C | 0.3 | - | 1.90 | 18 |
| $MoS_2$/RGO | 0.1 | - | 1.90 | |
| $MoS_x$-CB | 0.5 | - | 1.86±0.03 | 19 |
| $Mo_3S_{13}$-CB | 0.5 | - | 1.81±0.03 | |
| | 1 | - | 1.95 | |
| electrodeposited $MoS_x$ | 0.38 | - | $1.90^{(**)}$ | 20 |
| $FeS_2$/C | 0.5 | - | 2.00 | 21 |
| | 1 | - | 2.10 | |

In all cases, MEAs were prepared using Nafion membrane and Ir-based anode catalyst.
$^{(**)}$ PEM electrolyzer working at 90°C
C and CB – carbon black, RGO – reduced graphene oxide, CC – carbon cloth

## References


(1) Tran, P. D.; Tran, T. V.; Orio, M.; Torelli, S.; Truong, Q. D.; Nayuki, K.; Sasaki, Y.; Chiam, S. Y.; Yi, R.; Honma, I.; Barber, J.; Artero, V., Coordination polymer structure and revisited hydrogen evolution catalytic mechanism for amorphous molybdenum sulfide. *Nat. Mater.* **2016,** *15* (6), 640-647.

(2) Li, Y.; Yu, Y.; Huang, Y.; Nielsen, R. A.; Goddard, W. A.; Li, Y.; Cao, L., Engineering the composition and crystallinity of molybdenum sulfide for high-performance electrocatalytic hydrogen evolution. *ACS Catal.* **2015,** *5* (1), 448-455.

(3) Pham, K.-C.; McPhail, D. S.; Wee, A. T. S.; Chua, D. H. C., Amorphous molybdenum sulfide on graphene–carbon nanotube hybrids as supercapacitor electrode materials. *RSC Adv.* **2017,** *7* (12), 6856-6864.

(4) Nguyen, D. N.; Nguyen, L. N.; Nguyen, P. D.; Thu, T. V.; Nguyen, A. D.; Tran, P. D., Crystallization of amorphous molybdenum sulfide induced by electron or laser beam and its effect on $H_2$-evolving activities. *J. Phys. Chem. C* **2016,** *120* (50), 28789-28794.

(5) Guo, X.; Wang, Z.; Zhu, W.; Yang, H., The novel and facile preparation of multilayer $MoS_2$ crystals by a chelation-assisted sol–gel method and their electrochemical performance. *RSC Adv.* **2017,** *7* (15), 9009-9014.

(6) Li, Y.; Nakamura, R., Structural change of molybdenum sulfide facilitates the electrocatalytic hydrogen evolution reaction at neutral pH as revealed by in situ Raman spectroscopy. *Chinese J. Catal.* **2018,** *39* (3), 401-406.

(7) Khai, T. V.; Long, L. N.; Phong, M. T.; Kien, P. T.; Thang, L. V.; Lam, T. D., Synthesis and Optical Properties of $MoS_2$/Graphene Nanocomposite. *J. Electron. Mater.* **2020,** *49* (2), 969-979.

(8) Sun, Z.; Yang, M.; Wang, Y.; Hu, Y. H., Novel binder-free three-dimensional $MoS_2$-based electrode for efficient and stable electrocatalytic hydrogen evolution. *ACS Appl. Energy Mater.* **2019,** *2* (2), 1102-1110.

(9) Alemán-Vázquez, L. O.; Torres-García, E.; Villagómez-Ibarra, J. R.; Cano-Domínguez, J. L., Effect of the particle size on the activity of $MoO_xC_y$ catalysts for the isomerization of heptane. *Catal. Lett.* **2005,** *100* (3), 219-226.

(10) Hao, Z.; Yang, S.; Niu, J.; Fang, Z.; Liu, L.; Dong, Q.; Song, S.; Zhao, Y., A bimetallic oxide $Fe_{1.89}Mo_{4.11}O_7$ electrocatalyst with highly efficient hydrogen evolution reaction activity in alkaline and acidic media. *Chem. Sci.* **2018,** *9* (25), 5640-5645.

(11) Zhang, W.; Shi, S.; Zhu, W.; Yang, C.; Li, S.; Liu, X.; Hu, N.; Huang, L.; Wang, R.; Suo, Y.; Li, Z.; Wang, J., In-situ fixation of all-inorganic Mo–Fe–S clusters for the highly selective removal of lead(II). *ACS App. Mater. Interfaces* **2017,** *9* (38), 32720-32726.

(12) Di Giovanni, C.; Wang, W.-A.; Nowak, S.; Grenèche, J.-M.; Lecoq, H.; Mouton, L.; Giraud, M.; Tard, C., Bioinspired iron sulfide nanoparticles for cheap and long-lived electrocatalytic molecular hydrogen evolution in neutral water. *ACS Catal.* **2014,** *4* (2), 681-687.

(13) Song, M. J.; Hwang, S. W.; Whang, D., Non-enzymatic electrochemical CuO nanoflowers sensor for hydrogen peroxide detection. *Talanta* **2010**, 80, 1648-1652.

(14) Krejci, J.; Sajdlova, Z.; Nedela, V.; Flodrova, E.; Sejnohova, R.; Vranova, H.; Plicka, R., Effective surface area of electrochemical sensors. *J. Electrochem. Soc.* **2014**, 161, B147-B150.

(15) Ameur, Z. O.; Husein, M. M., Electrochemical behavior of potassium ferricyanide in aqueous and (w/o) microemulsion systems in the presence of dispersed nickel nanoparticles. *Sep. Sci.Technol.* **2013**, 48:5, 681-689.

(16) Antolini, E., Carbon supports for low-temperature fuel cell catalysts. *Appl. Catal. B: Environ.* **2009,** *88* (1), 1-24.

(17) Hoogers, G., *Fuell Cell Technology Handbook*. CRC Press UC, Boca Raton: **2003**.

(18) Corrales-Sánchez, T.; Ampurdanés, J.; Urakawa, A., $MoS_2$-based materials as alternative cathode catalyst for PEM electrolysis. *Int. J. Hydrogen Energy* **2014,** *39* (35), 20837-20843.
(19) Ng, J. W. D.; Hellstern, T. R.; Kibsgaard, J.; Hinckley, A. C.; Benck, J. D.; Jaramillo, T. F., Polymer electrolyte membrane electrolyzers utilizing non-precious Mo-based hydrogen evolution catalysts. *ChemSusChem* **2015,** *8* (20), 3512-3519.
(20) Kim, J. H.; Kim, H.; Kim, J.; Lee, H. J.; Jang, J. H.; Ahn, S. H., Electrodeposited molybdenum sulfide as a cathode for proton exchange membrane water electrolyzer. *J. Power Sources* **2018,** *392*, 69-78.
(21) Giovanni, C. D.; Reyes-Carmona, Á.; Coursier, A.; Nowak, S.; Grenèche, J. M.; Lecoq, H.; Mouton, L.; Rozière, J.; Jones, D.; Peron, J.; Giraud, M.; Tard, C., Low-cost nanostructured iron sulfide electrocatalysts for PEM water electrolysis. *ACS Catal.* **2016,** *6* (4), 2626-2631.